FE MODEL OF A CORD-RUBBER RAILWAY BRAKE TUBE SUBJECTED TO EXTREME OPERATIONAL LOADS ON A REVERSE CURVE TEST TRACK

Gyula Szabó, Károly Váradi
Department of Machine and Product Design
Budapest University of Technology and Economics
1-3 Műegyetem rkp., Budapest 1111, Hungary
E-mail:szabo.gyula@gt3.bme.hu

KEYWORDS
filament-wound composite tube, cord-rubber tube, railway brake tube, FE model, sub-zero temperature, reverse curve, draw and buffing gear interaction test

ABSTRACT

In certain cases, rolling stocks and railway vehicle components, i.e. brake tubes need to operate under extreme conditions such as at sub-zero temperature (e.g. -40°C) and on a reverse curve track, when displacements of the suspension points of the tubes cause large deformations in tubes.
In this paper, displacements of the suspension points of the tubes are determined by a kinematic model validated by a draw and buffing gear test [1]. Afterwards, FE simulation has been carried out at minimum and maximum suspension point distance based on these displacements for the investigation of stress, strain states and possible failure considering the case of internal pressure and no internal pressure.
Equivalent strain, stress and Tsai-Hill failure indices are much below the criterial values, so failure is not probable.
The straight section between the curves of opposite curvatures reduces deformation in tubes in the critical positions leading to lower strain, stress and failure index values.

INTRODUCTION

Cord-rubber composite tubes are widely used in applications where relatively high loads need to be withstood with low dead load, and very large deformations occur. These brake tubes are produced mainly by filament-winding due to high fiber precision and good automation capability with low tooling costs [2]. Winding angle of cords is usually ±55° making filament-wound tubes optimal to biaxial tension (when the loads are uniaxial tension and internal pressure) [3]. Filament-wound cord-rubber tubes also find extensive use in railway transportation as railway brake tubes due to their high strength-to-weight ratio, high flexibility and corrosion resistance. Cord-rubber tubes installed on railway carriages can be seen in Figure 1.

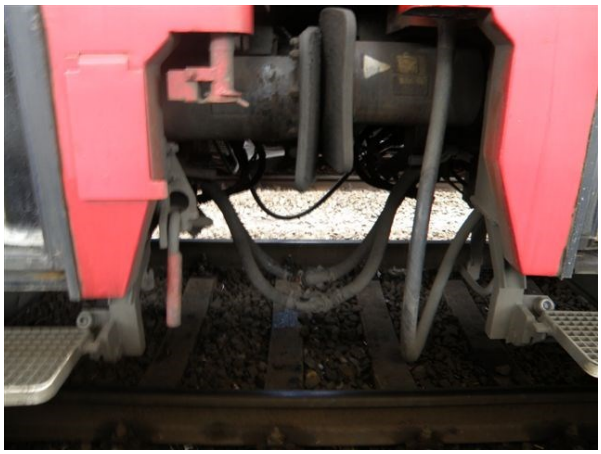

Figure 1. Railway brake tubes installed on railway carriages

Operation on reverse curve tracks (when both rolling stocks are on curves of opposite curvatures) induce large displacement of the suspension points of the brake tubes thus leading to large deformation of the tubes. However, deformation is impeded at sub-zero temperatures (e.g. -40°C) due to the elevated stiffness of the material therefore bringing about higher stresses than at room temperature.

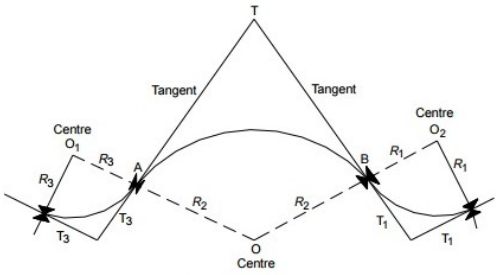

Figure 2. Schematic representation of a reverse curve track [4]

Schematic depiction of a reverse curve can be seen in Figure 2. A reverse curve (also known as S-curve) consists of curves having opposite curvatures.These curves are connected to one another by a transition curve or a straight line. The length of the straight line between the two curves is usually more than 30 m in high-speed applications although the connecting straight lines can be much shorter on maintenance tracks, being

Communications of the ECMS, Volume 35, Issue 1,
Proceedings, ©ECMS Khalid Al-Begain, Mauro Iacono,
Lelio Campanile, Andrzej Bargiela (Editors)
ISBN: 978-3-937436-72-2 / 78-3-937436-73-9(CD) ISSN 2522-2414

a worse case regarding the operational conditions because displacements of the suspension points of the tubes are larger-even though operation on maintenance tracks is not considered in railway rolling stock design practice. [4]
In traditional railway transportation (non-high speed applications), the minium curve radius is 150 m and an intermediate straight section of 6 m must be placed between the curves of opposite curvatures to ensure vehicle stability. In this case, track gauge is 1470 mm. [5].
The aim of this article is to investigate deformation, stress and strain states and possible failure of cord-rubber railway brake tubes subjected to bending and torsion due to operation on an S-curve at -40°C. Materials and methods are similar to those used in [6], however, the railway test track is different which has a significant effect on displacements of the suspension points of the tubes, and thus on the resulting strain and stress states. Furtmore, in this paper, validation of the kinematic simulation has been performed additionally based on [1].

DRAW AND BUFFING GEAR INTERACTION TEST [1]

Railway rolling stock manufactured in the European Union needs to fulfil the requirements of LOC&PAS TSI [7], so draw and buffing gear interaction test [1] of a coach manufactured by MÁV-Start Zrt (Hungarian State Railways) had to be performed. The test was carried out by MÁV Central Rail And Track Inspection Ltd. (MÁV KFV Kft.) on the Szolnok Railway Maintenance Site of MÁV in Szolnok, Hungary between 16 June 2019 and 20 June 2019 on a purpose-built reverse curve test track with a nominal curve radius of 150 m. Length of the vehicle body has been 26100 mm, distance of the bogie pivots has been 19 000 mm, bogie type was Siemens SF 400. Tests were conducted at a speed of 5km/h so that forces exerted by the traction vehicle did not influence the measurements. [1]

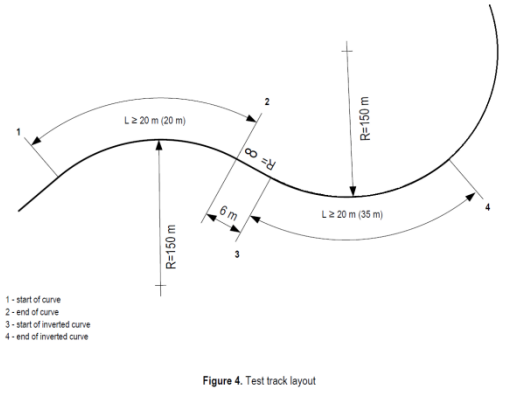

Figure 3. Test track layout [1]

The test track is illustrated in Figure 3. It consists of an initial tangent (straight) section before 1, a 20 m long curve with a radius of 150 m (between 1 and 2), an intermediate straight section of 6 m (between 2 and 3), a 35 m long curve with a radius of 150 m (between 3 and 4) and a curved section after 4 with an approximate radius of 150 m. The test (pulled run is considered hereinafter) commenced at point 1 and lasted until the rear coach has passed point 4.

Figure 4 shows the displacement-type measured quantities. X_1 is the buffer compression on the left side, x_2 is the buffer compression on the right side, whereas y_1 is the lateral deviation at the coupled end (Figure 4).

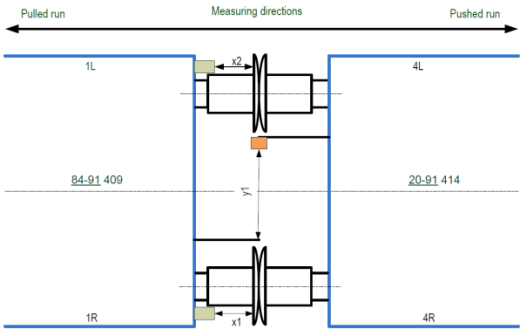

Figure 4. Location of the applied sensors [1]

Lateral displacement y_1 has been used for the validation of the kinematic simulation. It has been measured by a draw-wire displacement sensor as it can be seen in Figure 5. Lateral displacement results can be seen in Figure 6 as a function of measurement time.

Figure 5. Draw-wire displacement sensor utilized for the measurement of lateral displacement y_1.

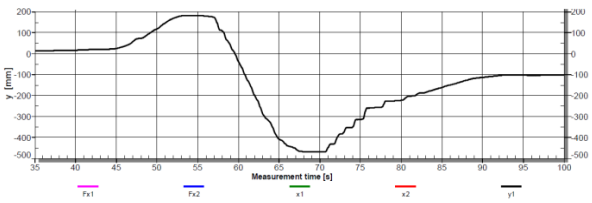

Figure 6. Lateral displacement y_1 as a function of time

KINEMATIC SIMULATION

Kinematic simulation has been performed in PTC Creo 2.0 Mechanism environment based on the dimensions of the draw and buffing gear interaction test. The kinematic model along with the railway track is shown in Figure 7. The purpose of the kinematic model is to obtain the positions of the suspension points of the positioning pins of the tubes at critical cases (minimum and maximum suspension point distance) in order to determine the displacements of these suspension points required for the FE model.

Figure 7. Representation of the railway track in the kinematic model

The assembly can be seen with its constraints in Figure 8. The dimensions (Figure 9) are in accordance with railway standards [8,9] and the test report [1].The railway track is grounded, to which bogies are attached by *slot* constraints at the railway wheels. Bogies and carriages are connected by *pin* contacts at the bogie pivots, which permit only rotational displacement around their axes. Carriages are connected to one another by *the draw gear*, which is able to rotate around fix points on the carriages (represented as *pin* contacts). The assembly is driven by a servo motor attached to one of the slot constraints on the rightmost bogie (Figure 8). [6]
The assembly contains the control points on both carriages required for the validation of the kinematic simulation (Figure 8).

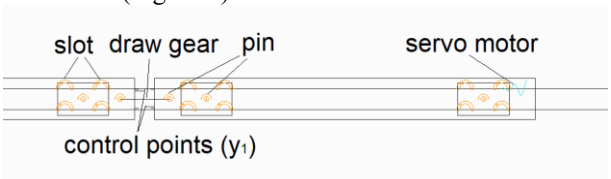

Figure 8. Schematic representation of the kinematic model along with constraints

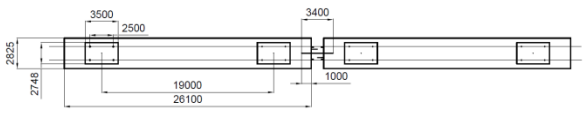

Figure 9. Schematic drawing of the kinematic model with dimensions

Relative displacements of the control points (Figure 8) can be seen as a function of time in Figure 10. Comparing results of the kinematic simulation with results of the draw and buffing gear test (Figure 10 and Figure 6 respectively), a considerably good agreement can be observed. The two curves have the same tendencies and the periodicity is nearly identical. However there is a minor difference in terms of the extremums, (the maximum lateral displacement is 312 mm instead of 200 mm and the minimum lateral displacement is -576 mm instead of approximately -470 mm), this can be attributed to several factors that could not be taken into account in the simulation.
In the test train, there are clearances in the subassemblies, and there is a slight lag in the movement of the bogie pivots.

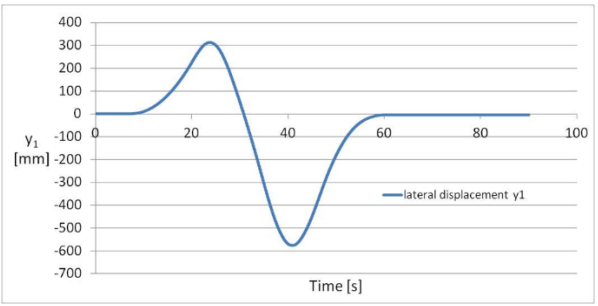

Figure 10. Lateral displacement (y_1)-time

Results of the kinematic model is necessary to estimate the displacements of the suspension points of the positioning pins of the tubes that govern the movement of the tubes [6]. Below, the left pair of tubes is considered.
At the start of the simulation, distance of the suspension points is 840 mm, which firstly diminishes because of being on the inner side of the first curve, until a minimum of 770 mm. Then, the distance increases as the bogies of the first coach begin to negotiate the second curve. After reaching the maximum of 985 mm, the bogies of the second coach get on the second track and the distance between the suspension points of the tubes slightly decreases. The extremums are considered as worst cases regarding the positions of the tubes [6].

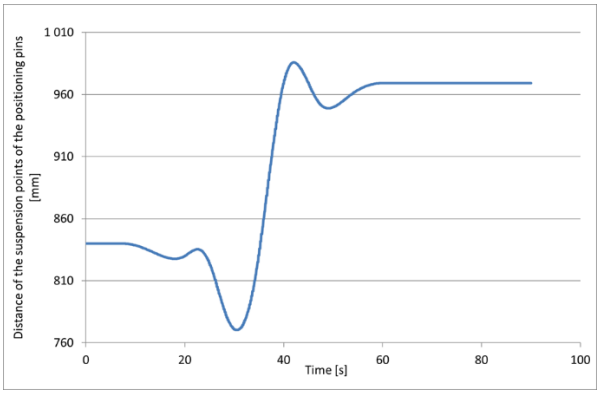

Figure 11. Distance of the suspension points of the positioning pins as a function of simulation time

Minimum and maximum suspension point distances are illustrated in Figure 12 and Figure 13 respectively.

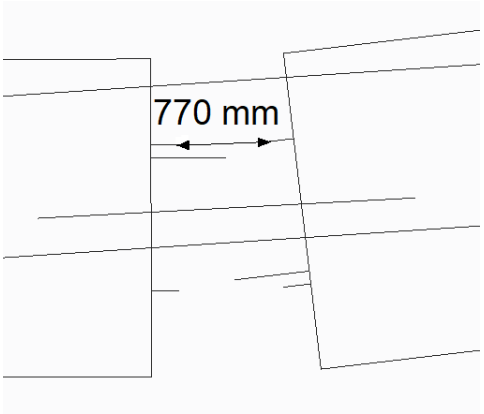

Figure 12. Railway cars at the moment of minimum suspension point distance

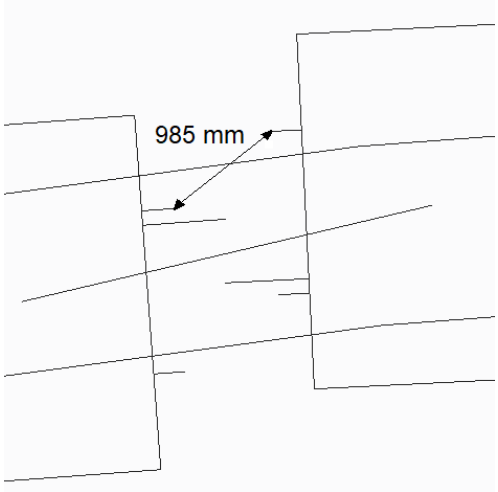

Figure 13. Railway cars at the moment of maximum suspension point distance

The displacements of the suspension points of the tubes in the FE model (see Table 1) have been calculated based on the positions acquired from the kinematic model (Figure 12, Figure 13).

FE MODEL [6]

The objective of the FE simulation is to gain strain, stress and Tsai-Hill failure index distributions for the assessment of failure at -40°C and the prescribed displacements derived from the kinematic simulation on the reverse curve track.

The FE model consists of two tubes and positioning pins on the two sides of the tubes used for actuating the tubes and positioning pins needed to connect the tubes.

Each tube is 620 mm long, consisting of an inner rubber liner, reinforcement layers and an outer rubber liner, shown in Figure 14. The layup is [+55°/-55°/+55°/-55°] and the material coordinate system of the tube is cylindrical.

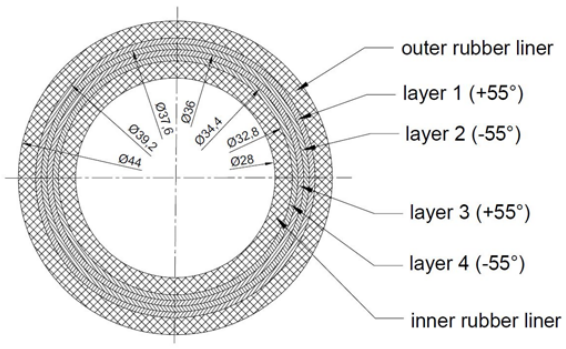

Figure 14. Cross-section of the tube [10]

Material model of the reinforcement layers is transversely isotropic, being a special case of orthotropy. Material properties have been calculated by utilizing the formulae of rules of mixture [11] based on the material properties of the components and fiber volume fraction. Material properties are considered *at -40°C*.

Material properties of the reinforcement layers are the following: modulus of elasticity of fibre is E_f=2961 MPa, Poisson's ratio of fibre is supposed to be υ_f=0.2, modulus of elasticity of rubber matrix is $E_m=E_r$= 19.1 MPa. E_1=1345 MPa, $E_2=E_3$=57 MPa, $\upsilon_{12}=\upsilon_{13}$=0.3637, υ_{23}=0.496, $G_{12}=G_{23}=G_{13}$=19 MPa. Rubber liners, made of EPDM-EVA compound, regarded as incompressible, have been described by a 2 parameter Mooney-Rivlin model with parameters C_{10}=3.34 MPa, C_{01}=1.077 MPa, D=0 1/MPa. These material properties have been validated previously by uniaxial tensile tests performed on test specimens and tube pieces [12] and deflection test carried out at -40°C. [6]

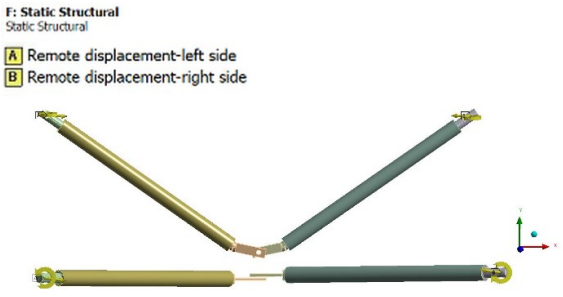

Figure 15. Prescribed displacements in the front view and in top view [6]

Actuation of the tubes is performed by prescribed displacements (Figure 15) of the suspension points of the positioning pins based on the kinematic simulation. The tubes are connected to each other in the middle by a fixed joint of holes of two positioning pins, whose distance is 10 mm in direction Z (see Figure 15).

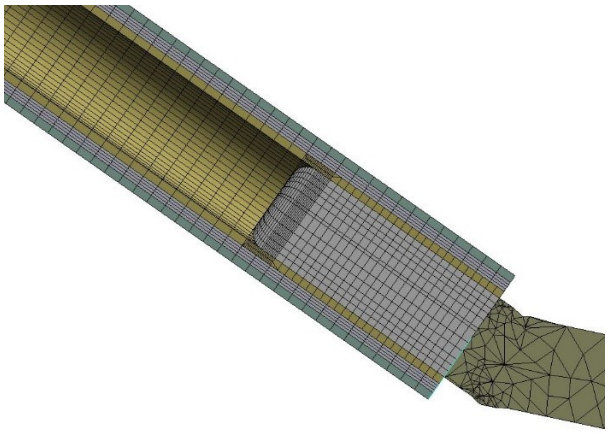

Figure 16. Meshed FE model [6]

The Finite Element model consists of 151548 nodes, 110800 SOLID185 hexahedral elements and 50260 SOLID 187 tetrahedral elements, a detail of the mesh can be seen in Figure 16. (The positioning pin consists of two bodies, bonded to one another, due to meshing considerations.)
At the beginning of the FE simulation (t=0 s), the distance of the suspension points of the positioning pins is 1140 mm. Prescribed displacements for minimum and maximum suspension point distance load cases are listed in Table 1 relative to the initial configuration.

Table 1. Prescribed displacements of FE model without internal pressure

	translation X [mm]	translation Z [mm]	rotation Y
min. s. p. d. left	184.86	0	3.41
min. s. p. d. right	-184.86	0	-3.41
max. s.p. d. left	163.5	278.5	1.55
max. s. p. d. right	-163.5	-278.5	-1.55

where *min. s. p. d. left* is the abbreviation of minimum suspension point distance load case-left remote point
max. s. p. d. right is the abbreviation of maximum suspension point distance load case-right remote point

The load case of additional internal pressure in case of the minimum and maximum suspension point distances has been further investigated (Figure 17). By utilizing the symmetry of the model, in these examinations, only a half model has been examined (the left tube and its pins). The pressure load is 5 bar, the displacement of the connecting remote point (in the middle) and the displacement of the suspension point of the positioning pin match those of the displacement results of the simulation without internal pressure. This simulation consists of two time steps. In the first one, an internal pressure of 5 bar is applied to the inner lateral surface of the tube, while in the second one, the prescribed displacement results are applied.

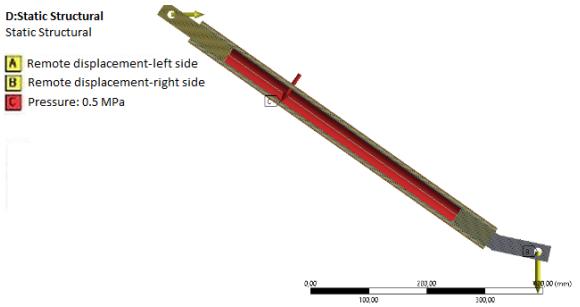

Figure 17. Half FE model with internal pressure [6]

Failure behaviour has been analysed with Tsai-Hill failure criterion. Tsai-Hill criterion is widely utilized for describing failure behaviour of cord-rubber composites [6, 13].
Strength properties in material directions are as follows: $X_t=X_c=342.5$ MPa , $Y_t= Y_c=Z_t= Z_c=34.2$ MPa (assuming strength is much lower in transverse directions); Q=R=S=5.5 MPa, derived from the strength of the rubber at -40°C (half of the strength of the rubber) [6]

RESULTS

RESULTS WITHOUT INTERNAL PRESSURE

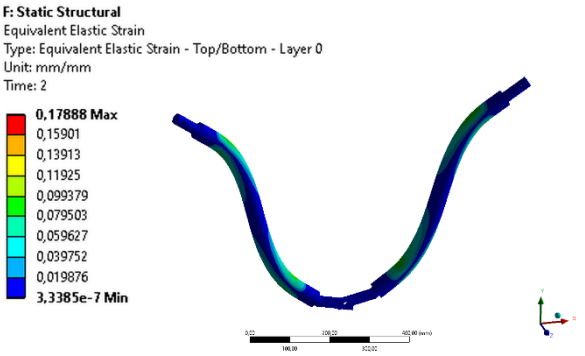

Figure 18. Equivalent strain at minimum suspension point distance (deformation scale 1:1)

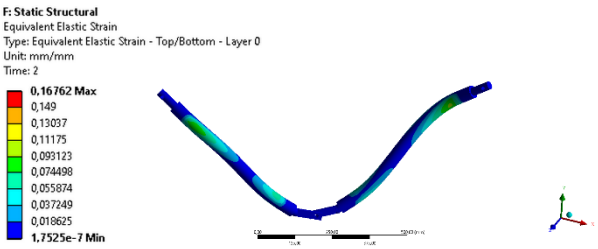

Figure 19. Equivalent strain at maximum suspension point distance (deformation scale 1:1)

Figure 18 shows equivalent strain results at minimum suspension point distance, while Figure 19 shows equivalent strains at maximum suspension point distance. In both cases, maximum equivalent strains are

below 0.2 and are considered as insignificant compared to the elongation at break of the rubber at -40°C, which is 90%.

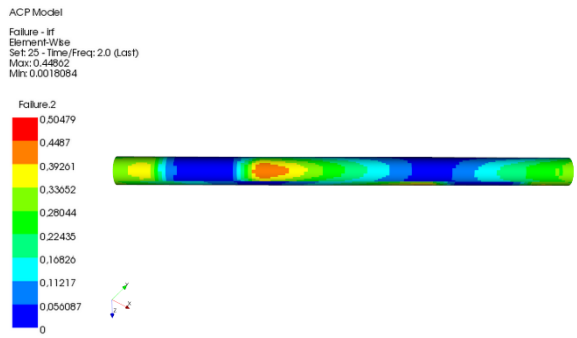

Figure 20. Tsai-Hill failure index distribution at minimum suspension point distance

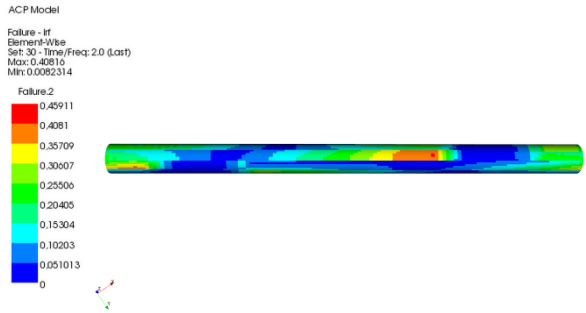

Figure 21. Tsai-Hill failure index distribution at maximum suspension point distance

Maximum failure indices are far below the criteria value of 1 in both minimum (0.45- shown in Figure20) and maximum suspension point distance (0.4- shown in Figure 21), so material failure is not probable in composite layers. These values are considerably lower than maximum values (0.54 and 0.62 respectively) presented in [6].

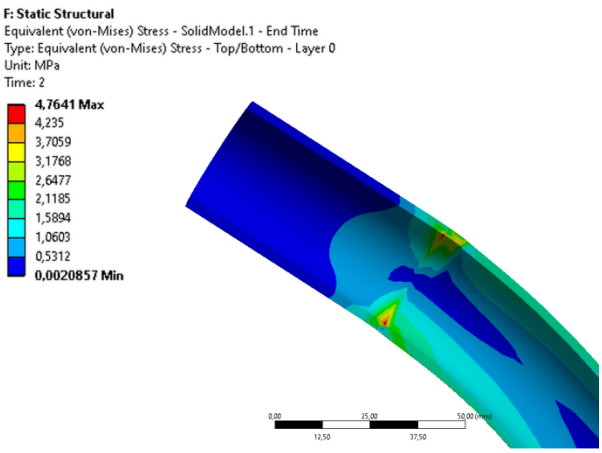

Figure 22. Equivalent stress in the inner rubber liner at minimum suspension point distance

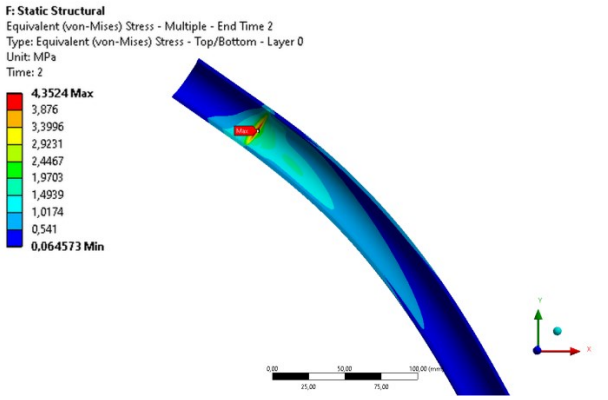

Figure 23. Equivalent stress in the inner rubber liner at maximum suspension point distance

As regards with rubber liners, maximum values arise in the inner rubber liner, at its contact surface with the positioning pin. Maximum values are nearly 4 MPa in both cases being much below the ultimate strength of the rubber at -40 °C (11 MPa).

RESULTS WITH INTERNAL PRESSURE

Tsai-Hill failure indices at minimum suspension point distance can be seen in Figure 24, while failure index values at maximum suspension point distance are shown in Figure 25. Maximum failure index at minimum suspension point distance is not influenced by internal pressure, while at maximum suspension point distance, maxium failure index is higher, although still much lower than the criterial value of 1.

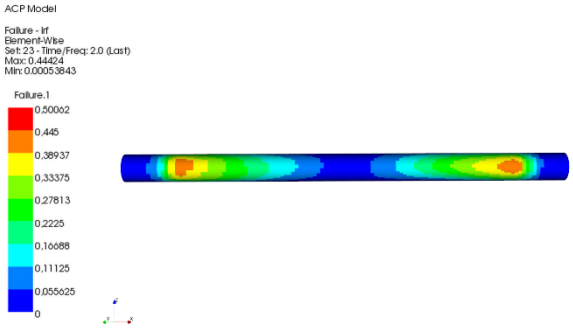

Figure 24. Tsai-Hill failure index distribution at minimum suspension point distance with internal pressure

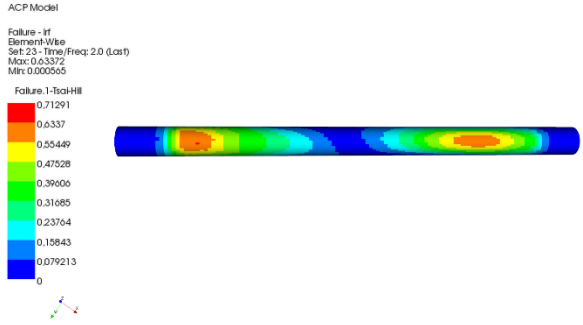

Figure 25. Tsai-Hill failure index distribution at maximum suspension point distance with internal pressure

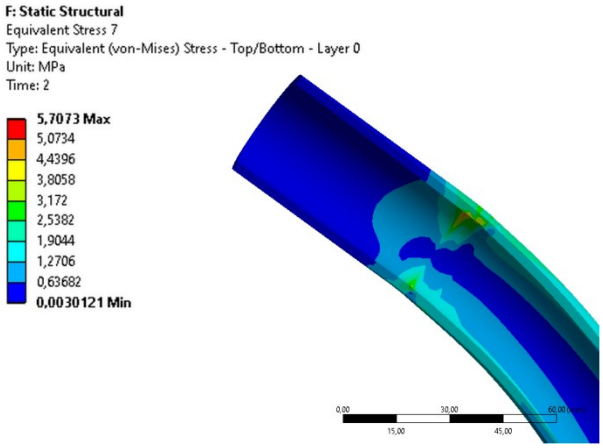

Figure 26. Equivalent stress in the inner rubber liner at minimum suspension point distance

Maximum equivalent stresses at minimum suspension point distance are shown in Figure 26, whereas maximum equivalent stresses at maximum suspension point distance are shown in Figure 27. Maximum stresses are slightly higher with internal pressure although the increase in stresses is not significant.

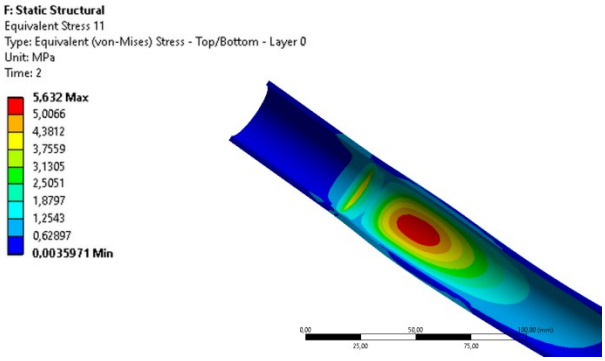

Figure 27. Equivalent stress in the inner rubber liner at maximum suspension point distance

CONCLUSIONS

Extreme operational loads have been considered in the FE model presented in this paper, firstly, because of the large deformations of the tubes as a result of operation on reverse curves and secondly because of stiffer material constants attributed to cold temperatures. Displacments of the suspension points have been determined based on a kinematic simulation validated by a draw and buffing gear interaction test. The utilization of the geometry of the test track led to more realistic carriage positions at minimum and maximum suspension point distance than the positions presented previously in [6]. The existence of a straight section between the curves of opposite curvature makes extrmemums of suspension point distances closer to the initial value (maximum gets lower while minimum gets higher). This also reduces loads arising in the tubes leading to considerably lower maximum stresses and Tsai-Hill failure indices than stresses and Tsai-Hill failure indices reported in [6].

The material properties of the composite layers and the rubber liners have been calculated at -40°C.

In rubber liners, equivalent strains are much below elongation at break (90%), equivalent stress values are also much lower than ultimate tensile strength (11 MPa) and high values are confined to a relatively small zone, so failure is not probable in liners. In composite layers, Tsai-Hill failure indices are also below the criterial value of 1, so failure is not likely in composite layers either.

ACKNOWLEDGEMENT

Authors would like to express their gratitude to Dr. Attila Piros, Department of Machine and Product Design at the Budapest University of Technology and Economics for his valuable help regarding the formulation of the kinematic model.

Authors are also extremely grateful to MÁV Central Rail and Track Inspection Ltd., namely to Csaba Pálfi, for providing them with test report 7420007-19/VÜE-1VJ-1.0-EN.

The research reported in this paper and carried out at BME has been supported by the NRDI Fund (TKP2020 NC, Grant No. BME-NCS) based on the charter of bolster issued by the NRDI Office under the auspices of the Ministry for Innovation and Technology.

REFERENCES

[1] Test report 7420007-19/VÜE-1VJ-1.0-EN, MÁV Central Rail and Track Inspection Ltd.

[2] Mallick, P. K., (1997) Composites Engineering Handbook, CRC Press, , ISBN 9780824793043

[3] Soden PD, Kitching R, Tse PC. (1989) Experimental failure
stresses for ±55° filament wound glass fibre reinforced plastic tubes under biaxial loads Composites; 20 (2): 125–135. DOI: https://doi.org/10.1016/0010-4361(89)90640-X

[4] Railway Engineering: Compound and reverse curve http://www.brainkart.com/article/Railway-Engineering--Compound-and-Reverse-Curve_4228/

[5] UIC 527-1 Coaches vans and wagons-Dimensions of buffer heads- Track layout on S-curves, 2005

[6] Szabó, G and Váradi, K. (2019) FE simulation of a cord-rubber composite tube subjected to bending due to operation on railway track with extremely low curve radius at sub-zero temperature, Proceedings - European Council for Modelling and Simulation, ECMS, 33 (Caserta, Italy,) No. 1, 377-383

[7] Commission Regulation (EU) No. 1302/2014 concerning a technical specification for interopera-bility relating to the 'rolling stock — locomotives and passenger rolling stock' subsystem of the rail system in the European Union (LOC & PAS TSI

[8] UIC 541-1 Regulations concerning the design of break components

[9] UIC 520 -Wagons, coaches and vans-Draw gear-Standardisation

[10] Szabó, G., Váradi, K. and Felhős, D. 2017 Finite Element Model of a Filament-Wound Composite Tube Subjected to

Uniaxial Tension Modern Mechanical Engineering; 7 (4): 91–112. DOI:10.4236/mme.2017.74007
[11] Chawla, K. K. Composite Materials Science and Engineering (3rd Ed.). New York; London: Springer. 2009
[12] Szabó, G. and Váradi, K. 2018 Uniaxial Tension of a Filament-wound Composite Tube at Low Temperature, Acta Technica Jaurinensis, 11 (2), pp. 84-103. doi: 10.14513/actatechjaur.v11.n2.456
[13] Reddy, J.N., Soares C.A.M et al. Mechanics of Composite Materials and Structures, Springer. 1999

GYULA SZABÓ is a PhD Student at the Faculty of Mechanical Engineering, Budapest University of Technology and Economics. His research interests include finite element modelling, composites, particularly cord rubber tubes and diaphragms.
KÁROLY VÁRADI is a professor at the Department of Machine and Product Design, Budapest University of Technology and Economics. His research interests include finite element modelling, structural analyses, composites, fracture mechanics and biomechanics